

Progenitor Mass Distribution for 22 Historic Core-Collapse Supernovae

Mariangelly Díaz-Rodríguez,^{1*} Jeremiah W. Murphy,^{1†} Benjamin F. Williams,² Julianne J. Dalcanton² and Andrew E. Dolphin^{3,4}

¹*Department of Physics, Florida State University, Tallahassee, FL 32304, USA*

²*Department of Astronomy, Box 351580, University of Washington, Seattle, WA 98195, USA*

³*Steward Observatory, University of Arizona, Tucson, AZ 85719, USA*

⁴*Raytheon, Tucson, AZ 85734, USA*

Accepted 2021 June 13. Received 2021 May 24; in original form 2021 January 22

ABSTRACT

We infer the progenitor mass distribution for 22 historic core-collapse supernovae (CCSNe) using a Bayesian hierarchical model. For this inference, we use the local star formation histories to estimate the age for each supernova (SN). These star formation histories often show multiple bursts of star formation; our model assumes that one burst is associated with the SN progenitor and the others are random bursts of star formation. The primary inference is the progenitor age distribution. Due to the limited number of historic SNe and highly uncertain star formation at young ages, we restrict our inference to the slope of the age distribution and the maximum age for CCSNe. Using single-star evolutionary models, we transform the progenitor age distribution into a progenitor mass distribution. Under these assumptions, the minimum mass for CCSNe is $M_{\min} = 8.60_{-0.41}^{+0.37} M_{\odot}$ and the slope of the progenitor mass distribution is $\alpha = -2.61_{-1.18}^{+1.05}$. The power-law slope for the progenitor mass distribution is consistent with the standard Salpeter initial mass function ($\alpha = -2.35$). These values are consistent with previous estimates using precursor imaging and the age-dating technique, further confirming that using stellar populations around SN and supernova remnants is a reliable way to infer the progenitor masses.

Key words: stars: massive – supernovae: general – methods: statistical

1 INTRODUCTION

Stellar evolution predicts that single massive stars with initial masses $\gtrsim 8\text{--}11 M_{\odot}$ likely end their lives with core collapse, and a large fraction of them likely explode as a *core-collapse supernova* (CCSN; Woosley et al. 2002; Eldridge & Tout 2004; Smartt 2009). While there is some theoretical progress in understanding which stars explode and which collapse to form black holes, predicting which stars actually explode remains uncertain (Burrows & Goshy 1993; Murphy & Burrows 2008; Murphy & Dolence 2017; Mabanta & Murphy 2018; Ugliano et al. 2012; Sukhbold et al. 2016; Ebinger et al. 2018). Hence, it is important to constrain the theory by using observations to infer the progenitor mass distribution for these explosions.

Díaz-Rodríguez et al. (2018, hereafter DR18) used the stellar populations associated with 94 supernova remnants (SNRs) to infer the progenitor mass distribution. DR18 found that the minimum mass (M_{\min}) for CCSNe is $7.33_{-0.16}^{+0.02} M_{\odot}$, the maximum mass (M_{\max}) for explosion is greater than $59 M_{\odot}$, and the power-law slope in between is $\alpha = -2.96_{-0.25}^{+0.45}$; these represent the tightest constraints on the

progenitor mass distribution to date. The analysis assumed that SNRs are unbiased tracers of recent supernovae (SNe). However, SNe and SNRs represent two different tracers of SN location and using SNRs as SN tracers may lead to a biased sample. As a preliminary test of this bias, we infer the progenitor age distribution and progenitor mass distribution of 22 historic SNe.

Generally, there are two basic techniques to infer SNe progenitor masses. The first involves the direct identification of the precursor that led to an SN (e.g. Smartt et al. 2002a,b, 2004, 2009; Van Dyk et al. 2003a,b; Maund et al. 2004; Van Dyk et al. 2011, 2012a,b; Li et al. 2005, 2006, 2007; Maund et al. 2005, 2011, 2014; Hendry et al. 2006; Gal-Yam & Leonard 2009; Smartt 2009; Smith et al. 2011; Fraser et al. 2014); the other is age-dating the stellar populations associated with the SN. Estimating the initial mass of an SN precursor requires inferring the bolometric luminosity and temperature of the precursor and comparing to stellar evolution models to infer the progenitor mass (see Van Dyk 2017). While it is important to image the star that actually exploded, the direct imaging technique relies on the last, most uncertain stages of stellar evolution (Farrell et al. 2020).

Directly imaging the precursor has led to new constraints on the progenitors of CCSNe. One of the earliest progenitor

* E-mail: md14u@my.fsu.edu

† E-mail: jwmurphy@fsu.edu

studies found a minimum mass of $M_{\min} = 8.5^{+1.0}_{-1.5} M_{\odot}$ and a maximum mass of $M_{\max} = 16.5 \pm 1.5 M_{\odot}$ for 8 direct Type IIP SN progenitor detections and 12 upper limits (Smartt et al. 2009), assuming a progenitor distribution that matches the slope of the Salpeter initial mass function ($\alpha = -2.35$). As expected, all directly imaged progenitors of SN IIP are red supergiants (RSGs). The luminosity limit for observed RSGs in the local group is $\log(L/L_{\odot}) = 5.5$, and for single-star models this corresponds to an initial progenitor mass of $\sim 30 M_{\odot}$. The lack of detected high mass progenitors above $\sim 17 M_{\odot}$ (or luminosities above $\log(L/L_{\odot}) > 5.2$) in the progenitor sample in Smartt et al. (2009) suggested that the most massive RSGs may not be exploding as SN IIP. Later, in an updated and extended sample, Smartt (2015) again found that there were no RSGs above $\sim 17 M_{\odot}$.

Since this original suggestion of a red supergiant problem, a debate has developed about the statistical robustness of this result (see Walmswell & Eldridge 2012; Davies & Beasor 2018; Beasor & Davies 2016). For example, Davies & Beasor (2018) revisited the bolometric correction and other sources of systematics in Smartt et al. (2009) and Smartt (2015). They found a higher upper mass limit of $M_{\max} = 19.0^{+2.5}_{-1.3} M_{\odot}$, with a 95 % confidence limit of $< 27 M_{\odot}$. Based on their study, they concluded that the evidence for a population of ‘missing’ stars had only a minor statistical significance. More recently, Kochanek (2020) used a Bayesian approach to re-analyze the sample used by Smartt (2015) and Davies & Beasor (2018), finding a maximum mass of $M_{\max} = 19.01^{+4.04}_{-2.04} M_{\odot}$. This study used a one-sigma discrepancy to conclude that the red supergiant problem remains. However, Colquhoun (2014) conclude that in practical studies, uncertainties are often underestimated and that even a two-sigma discrepancy is wrong 30% of the time. They show that in practice, one needs to use the three-sigma rule to keep the false discovery rate under 5% (Colquhoun 2014). Hence, the conclusion that red supergiant problem remains is premature given that the Kochanek (2020) result is less than two sigma away from the expected upper limit of 25-30 M_{\odot} for RSGs (Smartt et al. 2009). In fact, these analyses are complicated by the many assumptions in the likelihood models selected; given these assumptions, it is easily possible for the uncertainties to be much larger than inferred.

More recently, Davies & Beasor (2020) propose a simpler statistical test. Given the observed RSG brightness distribution and that one is drawing a small sample, they calculate the probability of the brightest observed RSG being $\log(L/L_{\odot}) = 5.24 \pm 0.08$ (progenitor of SN S009hd) given that the true theoretical brightness limit is $\log(L/L_{\odot}) = 5.5$. They found that given the small number of observed progenitors to date, the current brightest SN IIP progenitor is consistent (with 95% confidence) with the observed RSG brightness distribution.

Considering the difficulty in obtaining large numbers of observed progenitors, there is a clear need for an alternative technique for inferring the progenitor mass distribution. While SN progenitors are usually visible as resolved stars in high-resolution images (Smartt 2009, 2015 and references therein), determining which progenitor explodes successfully remains uncertain because only a few progenitors have been discovered directly (Leonard 2010). This is either due to the discovery rate of SN progenitor stars in nearby galaxies or due to instrument limitations (e.g. depth, field of view). Cur-

rently, there are approximately only 30 direct detections and 38 upper limits, making the statistical constraints quite loose (Van Dyk 2017).

An alternative technique is to age-date the stellar population associated with the SN, and from this age, infer a mass. These age-dating techniques offer a way to increase the number of progenitor mass estimates (Maíz-Apellániz et al. 2004; Wang et al. 2005; Crockett et al. 2008; Gogarten et al. 2009; Vinkó et al. 2009; Badenes et al. 2009; Murphy et al. 2011, 2018; Williams et al. 2014; Williams et al. 2018; Maund 2017, 2018; Achetttl et al. 2019). This second technique to infer progenitor masses has the advantage in that it does not need a precursor image of the star before it exploded. Instead, it relies on age-dating the stellar populations in the vicinity of the star that exploded, which can be performed after the explosion.

The age-dating technique has been used to infer the progenitor masses of SNe (Panagia et al. 2000; Murphy et al. 2011; Williams et al. 2014; Williams et al. 2018) and SNRs (Badenes et al. 2009; Jennings et al. 2012, 2014; Díaz-Rodríguez et al. 2018; Achetttl et al. 2019). Previous studies includes deriving the progenitor mass for specific SNe (see Murphy et al. 2011; Williams et al. 2014; Murphy et al. 2018), whereas other studies used bigger samples to derive the overall progenitor mass distribution using the age-dating technique. For example, Jennings et al. (2012) studied 53 SNRs in M31 and found a M_{\min} between 7.0 – 7.8 M_{\odot} for a M_{\max} of $\sim 26 M_{\odot}$ and standard Salpeter IMF slope of $\alpha = -2.35$. In a later study, Jennings et al. (2014) used 115 SNRs in M31 and M33, and derived a progenitor mass distribution for CCSNe with a maximum mass of $M_{\max} = 35^{+5.0}_{-4.0} M_{\odot}$ and slope $\alpha = -2.35$; while assuming a minimum mass of $M_{\min} = 7.3 M_{\odot}$ as found previously in Jennings et al. (2012). On the other hand, they found a slope of $\alpha = 4.2^{+0.3}_{-0.3}$ when fixing the M_{\max} to 90 M_{\odot} . DR18 used Bayesian inference to infer all three parameters simultaneously using the SFHs for M33 (Jennings et al. 2014) and the SFHs for M31 (Lewis et al. 2015). DR18 found that the $M_{\min} = 7.33^{+0.02}_{-0.16} M_{\odot}$, the $M_{\max} > 59 M_{\odot}$, and the power-law slope in between is $\alpha = -2.96^{+0.45}_{-0.25}$ for 94 SNRs in M31 and M33. Using a similar age-dating technique, Achetttl et al. (2019) found a mass distribution that is consistent with a Salpeter IMF distribution using the stellar populations around 23 known SNRs in the Small Magellanic Cloud. Together, these age-dating techniques have increased the number of progenitor mass estimates by roughly a factor of ten.

While age-dating SNRs allows for a larger sample of progenitor mass estimates, there remains the possibility that the SNR catalogs are biased tracers of SNe. For example, DR18 found that the power-law slope for the progenitor mass is $\alpha = -2.96^{+0.45}_{-0.25}$, which is steeper than the standard Salpeter IMF. There are two interpretations of this steeper slope. Either the most massive stars are exploding less frequently, or there is a bias against finding SNRs in the youngest star formation (SF) regions. Comparing the progenitor mass distribution for SNe and SNRs would help to address whether SNR catalogs are biased.

In this paper, we infer the progenitor age distribution using the star formation histories (SFHs) around 22 historic SNe. We use a Bayesian inference framework previously derived in DR18 to infer the parameters of the distribution. In contrast to our previous study (DR18), we only infer the maximum

age (t_{\max}) and slope of the age distribution (β), while fixing the minimum age (t_{\min}) to 5.62 Myr. We then use stellar evolution models (Marigo et al. 2017) to translate the progenitor age distribution parameters to its counterpart in mass space.

An outline of the paper is as follows. In Section 2.1, we describe the SN sample used in this study. We then provide a summary of our Bayesian inference technique to infer the CCSN progenitor age distribution in sections 2.3 and 2.4. In section 3, we present the statistical results. In section 4, presents the conclusions and a discussion of our results in the context of previous progenitor analyses.

2 METHODS

2.1 SN Sample

We infer the age distribution for a total of 22 historic CCSNe within ~ 8 Mpc that also have high quality overlapping HST imaging (see Table 1). 11 of the supernovae (SNe) presented in this manuscript were published initially by Williams et al. (2014, hereafter W14) and the other 11 SNe are from an extended and updated study in Williams et al. (2018, hereafter W18). These historical CCSNe have of order arcsecond accuracy in their positions and modest foreground extinction. The authors used the *HST* archive to determine which CCSNe have imaging in two or more broadband filters in ACS, WFPC2 (WFC3 for the most recent SNe sample), or UVIS to cover as much region as possible of the host galaxies.

In Table 1, we include the SN names considered in this study, SN spectral type, host galaxy, number of stars in the photometry, etc. W14 and W18 used a combination of HSTphot and DOLPHOT (updated HSTphot (Dolphin 2000, 2016)) to obtain the photometry for each SN. See W14 and W18 for more information about exposure dates, durations, and depths for the SN sample.

2.2 Star Formation Histories

To infer the progenitor age distribution for these 22 SNe, we must estimate the age of the stellar populations near each SN. We use the SFH for the surrounding stellar population as this age estimate. The technique used to obtain the SFH for the sample in this study has been described and tested in several other studies. For example, Murphy et al. (2011) showed that applying this technique to SN2011dh is consistent with direct-imaging estimates, Jennings et al. (2014) derived the SFHs for 115 SNRs in M31 and M33, Gogarten et al. (2009) inferred the age and mass for an unusual transient in NGC 300, W18 inferred the progenitor masses for 25 Historic SNe, Murphy et al. (2018) estimated the age and mass for the black hole candidate N6946-BH1 and Williams et al. (2019) inferred the SFHs for 237 optically identified SNRs in M83.

Figures 1 and 2 show the SFHs for the 22 historic SNe sample used in this study. W18 inferred the SFH for each SN using Match 2.7 (Dolphin 2002, 2012, 2013). Match infers SFHs from observed color-magnitude diagrams (CMDs). W18 used the DOLPHOT package to calculate the photometry of all resolved stars within 50 pc of each SN. The same photometry package, in combination with HSTphot, was used to obtain the photometry for each SN from W14. Essentially, Match derives these SFHs by generating a set of theoretical

grids in color and magnitude using stellar evolution models of Girardi et al. (2010) and Marigo et al. (2017).

Match generates SFHs that most accurately represent the observed CMD of the region while taking into account the effects of observational errors, foreground extinction, and distance. While it is possible to fit a single isochrone to an observed CMD, due to the small numbers of massive stars and poor Poisson sampling of the upper end of the IMF, one can underestimate the turnoff mass (Williams et al. 2018). Essentially, Match fit superpositions of stellar populations to reproduce the observed CMD (Dolphin 2002; Gogarten et al. 2009; Jennings et al. 2012). As a result, the estimated recent SFH fits the turnoff and full luminosity function of the main sequence. Fitting the entire CMD and not just the turnoff adds significant statistical weight in age-dating the stellar population. The technique of using this fitting package and models has been tested against direct pre-cursor measurements and has shown to have a good agreement (e.g., Dolphin et al. 2003; Gallart et al. 2005; Williams et al. 2014; Williams et al. 2018, and many others). The work in this manuscript consists of using these SFHs to draw conclusion about the CCSNe theory, for more details about the CMD fitting see W18 and references therein. For a comparison of the 22 historic progenitor mass estimates used in this study, with those inferred using the direct imaging technique, see Figure 2 of W18.

The age-dating technique relies on the fact that the majority of stars are born clustered (Lada & Lada 2003) hence they have a common age ($\Delta t \lesssim 3 - 5 \text{ Myr}$) and metallicity (Bovy 2016). This is important, because stars that formed in common events remain physically nearby up to ~ 100 pc during the 100 Myr lifetimes. Hence, even after a star has exploded, the remaining stars still provide information about the age population and hence its mass. Previous similar studies has shown that this assumption is appropriate (e.g. Gogarten et al. 2009; Murphy et al. 2011; Jennings et al. 2014; Badenes et al. 2015; Sarbadhicary et al. 2017; Williams et al. 2019; Auchetti et al. 2019).

As DR18 note, there are three principal sources of uncertainty when inferring the age for each SN. First, the resolution of the SFH affects the accuracy for each age bin. The resolution for the SNe sample published in W14 is $\Delta \log_{10}(t/\text{Myr}) = 0.1$ and for the SNe in W18 is $\Delta \log_{10}(t/\text{Myr}) = 0.05$. Second, it is common to have multiple bursts of SF associated with the stellar population and we do not know which burst is due to the actual SNe explosion (see Figure 1 and 2). These multiple bursts usually contribute the most to the uncertainty in inferring the age for each object. Lastly, there is an uncertainty associated with the SF rate for each age bin. In a previous analysis, DR18 developed a technique to model the first two uncertainties: uncertainty due to resolution and due to multiple bursts. In this manuscript, we expand upon that work and develop a technique that models all three sources of uncertainties. In particular, we use a re-sampling method (Jackknife) to model the uncertainty in the SFH.

2.3 Hierarchical Bayesian Inference

To calculate the age distribution for the 22 historic SNe, we use Bayes' theorem to compute the posterior joint probability, $P(\theta|\text{Data})$, where θ represents the parameters of the

Table 1. SN sample^a used for this analysis.

SN	Type	R.A.	Dec.	Galaxy	Mpc	N_{stars}	Reference
SN1917A	II	308.69542	60.12472	NGC6946	6.8	52	W18
SN1923A	II P	204.28833	-29.85111	NGC 5236 (M83)	5.0	142	W14
SN1948B	II P	308.83958	60.17111	NGC 6946	6.8	201	W18
SN1951H	II	210.98042	54.36139	NGC 5457 (M101)	7.2	11	W14
SN1954A	Ib	183.9445833	36.2630556	NGC 4214	3.0	31	W18
SN1968D	II	308.74333	60.15956	NGC 6946	6.8	86	W18
SN1978K	II	49.41083	-66.55128	NGC 1313	4.1	19	W18
SN1980K	II L	308.875292	60.106597	NGC 6946	6.8	38	W18
SN1985F	Ib	190.38754	41.15164	NGC 4618	7.9	203	W18
SN1987A	II pec	83.86675	-69.26974	LMC	0.05	11800	W14
SN1993J	I Ib	148.85323	69.02047	NGC 3031 (M81)	4.0	143	W14
SN1994I	Ic	202.47530	47.19181	NGC5194	8.3	42	W14
SN2002ap	Ic pec	24.099375	15.753667	NGC 0628	10.0	5	W18
SN2002hh	II P	308.68454	60.12194	NGC 6946	6.0	66	W14
SN2003gd	II P	24.177708	15.738611	NGC 0628	10.0	20	W18
SN2004am	II P	148.94421	69.67725	NGC 3034 (M82)	4.0	37	W14
SN2004dj	II P	114.32092	65.59939	NGC 2403	4.0	127	W14
SN2004et	II P	308.85554	60.12158	NGC 6946	6.8	18	W18
SN2005cs	II P	202.47237	47.17450	NGC 5194	8.3	33	W14
SN2008bk	II P	359.46008	-32.55597	NGC 7793	4.0	248	W14
SN2008iz	II	148.96479	69.67939	NGC 3034 (M82)	4.0	56	W14
SN2017eaw	II P	308.684333	60.193306	NGC 6946	6.8	136	W18

Note.^a Columns are (1) name of SN, (2) SN spectral type, (3) right ascension of the SN, (4) declination of the SN, (5) host galaxy of the SN, (6) distance to the galaxy in Mpc, (7) the number of stars in the photometry within the physical radius of 50 pc, and (8) article reference. For more information about the SN sample see W18.

age distribution model. We assume that the SN progenitor age distribution is a power-law with an index of β and a minimum and maximum age (t_{min} and t_{max}). The posterior distribution is the probability of the model parameters given the observations:

$$P(\theta|\text{Data}) = \frac{\mathcal{L}(\text{Data}|\theta) P(\theta)}{P(\text{Data})} \propto \mathcal{L}(\text{Data}|\theta) P(\theta), \quad (1)$$

where $\mathcal{L}(\text{Data}|\theta)$ is the probability of observing the data, or also known as the likelihood function. $P(\theta)$ is the prior distribution and $P(\text{Data})$ is the posterior distribution normalization.

The primary source of data are a collection of CMDs of the resolved stars, one for each region surrounding an SN. Hence, our goal is to use Bayes' theorem to find the joint posterior distribution of the model parameters given the set of CMDs, $P(\theta|\{\text{CMD}\})$.

In this manuscript, we present a hierarchical Bayesian inference; the primary nuisance parameters are the SFHs derived by *Match*. For each CMD, *Match* infers the best-fit SFH and it uses a hybrid Monte Carlo (MC) algorithm to estimate a posterior distribution for the SFH, i.e. $P(\text{SFH}_k|\text{CMD}_k)$. Where the index k represents each SN. In this context, the formal hierarchical posterior distribution is

$$P(\theta|\{\text{CMD}_k\}) = \prod_k \int P(\theta|\text{SFH}_k) P(\text{SFH}_k|\text{CMD}_k) d\text{SFH}_k. \quad (2)$$

In principle, the basic steps to infer the age distribution parameters includes estimating $P(\theta|\text{SFH}_k)$, using the posterior distribution given by *Match*, $P(\text{SFH}_k|\text{CMD}_k)$, and marginalizing over these results via equation 2.

In DR18, $P(\text{SFH}_k|\text{CMD}_k)$ was essentially a delta function $\delta(\text{SFH}_k - \overline{\text{SFH}}_k|\text{CMD}_k)$, where $\overline{\text{SFH}}_k$ is the best fit SFH. Ideally, one would use the *hybridMC* results of *Match* for the distribution of SFH, $P(\text{SFH}_k|\text{CMD}_k)$. However, the approximate results of the *hybridMC* method and the highly uncertain SFHs presented problems in using this technique. For example, we calculated the median of the best-fit SFH and compared it to the distribution of medians from the *hybridMC* distribution. We found that the median best-fit was often an outlier in the *hybridMC* results. This shows that while the *hybridMC* results are an estimate for the distribution of SFH, for the low number of stars in our CMDs, they do not adequately represent $P(\text{SFH}_k|\text{CMD}_k)$.

Since we do not have an accurate estimate for $P(\text{SFH}_k|\text{CMD}_k)$, we use the data itself and a re-sampling method to estimate the effects of the uncertainties in the SFH. Two common re-sampling methods include the bootstrap and jackknife methods. The bootstrap method tends to work better for skewed distributions, while the jackknife tends to work better for small samples. Since the bootstrap double counts sources, this can affect the accuracy in inferring the posterior distribution for small samples. Alternatively, the jackknife method involves removing one data point exactly R times, where R is the number of data points, or in this case, the number of SNe. Therefore, the jackknife avoids the doubling counting problem.

For this analysis, the jackknife re-sampling method is as follows. The r th estimator for the posterior is

$$P_r(\theta|\{\text{CMD}_{k'}\}) = \int \prod_{k'} P(\theta|\text{SFH}_{k'}) P(\text{SFH}_{k'}|\text{CMD}_{k'}) d\text{SFH}_{k'}, \quad (3)$$

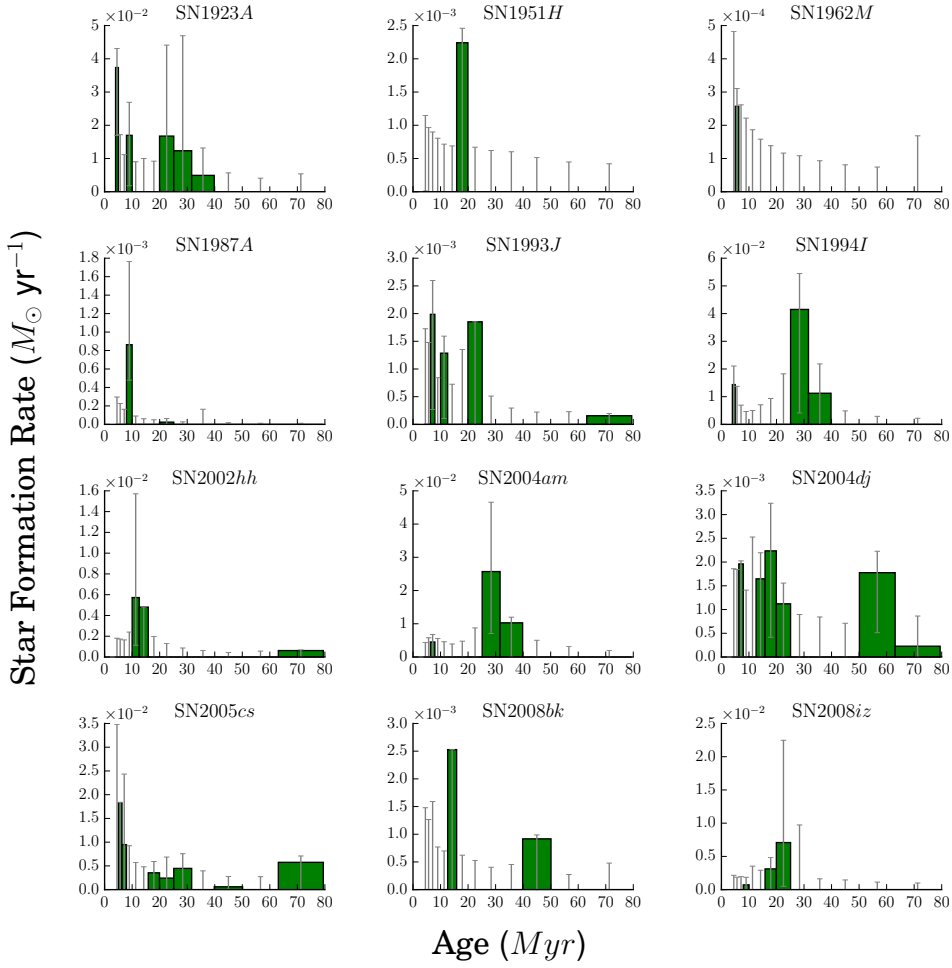


Figure 1. Differential star formation history (SFH) for 50-pc radius regions surrounding historic supernovae (SNe). The bars show the most likely SFH for each age bin, and the uncertainties show a 68% confidence interval from the hybrid-MCMC posterior. These 12 historical SNe are from W14. The easiest cases to interpret are when the SFH identifies one clear age (e.g. SN1951H, SN1962M, and SN1987A). In these cases, one may associate the age with the progenitor that exploded, and from that age, one may derive the corresponding mass. When there are multiple bursts of SF, it is not clear which burst is associated with the explosion. For these cases, we assume that only one burst is associated with the progenitor explosion; the others are random unassociated bursts of SF.

where k' represents the k' th SN of a subsample of SNe, and $P(\text{SFH}_{k'}|\text{CMD}_{k'}) = \delta(\text{SFH}_{k'} - \overline{\text{SFH}}_{k'}|\text{CMD}_{k'})$. Each re-sample r has a one less SN than the full sample, i.e. $N_{k'} = N_{\text{SNe}} - 1$. There are N_{SNe} unique subsamples for jackknife re-sampling, in other words $N_r = N_{\text{SNe}}$. To find the final posterior distribution, we marginalize over all of the jackknife estimators for the posterior.

$$P(\theta|\{\text{CMD}_k\}) \approx \sum_r^{N_{\text{SNe}}} P_r(\theta|\{\text{CMD}_{k'}\}). \quad (4)$$

The next section discusses the final piece, calculating $P(\theta|\{\text{SFH}_k\})$.

2.4 Inferring the Progenitor Age Distribution

The method to calculate the posterior distribution of θ given a set of SFHs, $P(\theta|\{\text{SFH}_{k'}\})$ is described in DR18. First, we convert each SN SFH into a probability density function (PDF) for the age, $P_{k'}(t)$. Match returns a discrete SFH, and the set of age bins is $\{i\}$, where i indexes each age bin. Given this discrete version of the SFH, the probability of a star being associated with age bin i is:

$$P_{\text{SFH}_{k'}}(i) = P_{k'}(i) \cdot \Delta t_{k',i} = \frac{\text{SFR}_{k'}(i)}{M_{\star,k'}(T_{\text{max}})} \cdot \Delta t_{k',i}. \quad (5)$$

This PDF is proportional to the stellar population SFR, the total amount of stars (M_{\star}) formed in the last T_{max} Myr, and Δt_i represents the width of each age bin i .

To accurately model and estimate the parameter t_{max} , we include ages above the predicted canonical value ($\sim 8 M_{\odot}$, this corresponds to an age of $\sim 45 \text{ Myr}$) in the single-star sce-

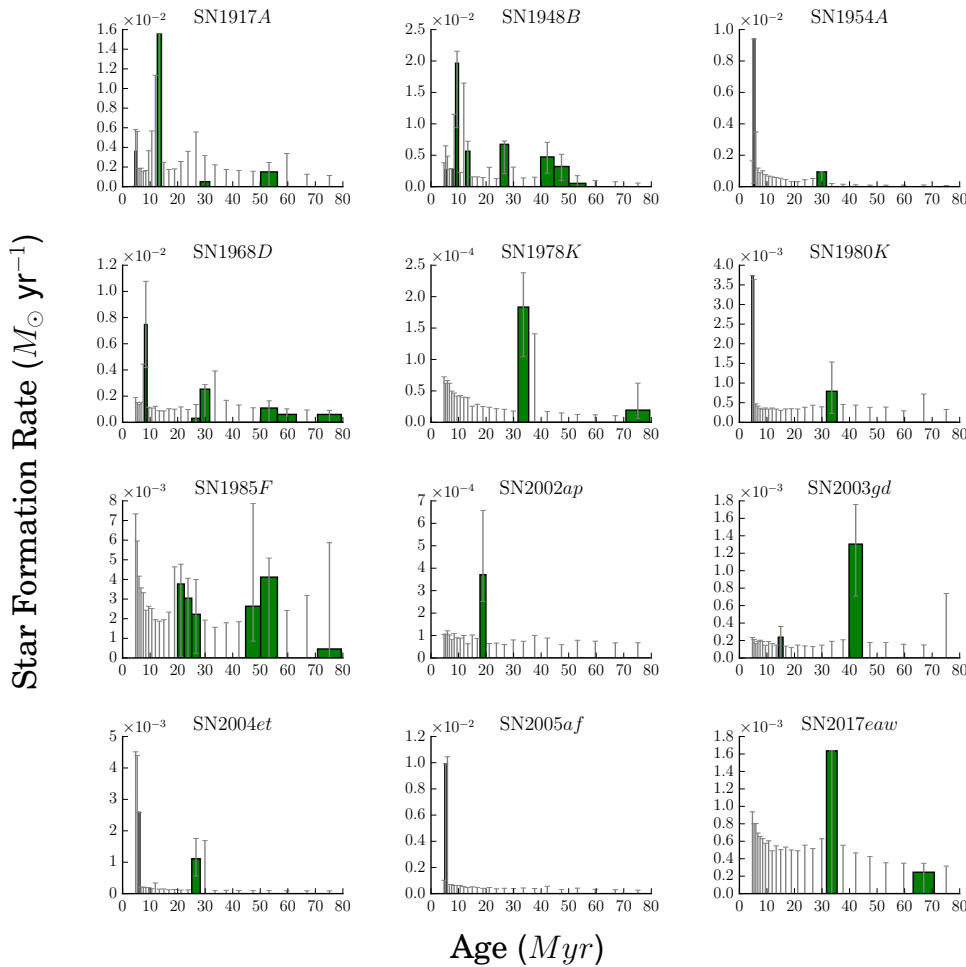


Figure 2. Same as Figure 1. These 12 historical SNe are from W18.

nario. To allow the algorithm to explore the parameter space fully, we consider ages from 5.62 Myr up to $T_{\max} = 80$ Myr. Figures 1 and 2 show the best-fit SFH with its corresponding uncertainties for our SN sample. In most cases, the best-fit SFH shows more than one burst of SF. Since it is not clear which burst is associated with the progenitor that exploded, one needs to model these unassociated bursts of SFH properly.

Figure 3, shows the stacked age distribution for all 22 SNe. To produce this stacked distribution, we sum the PDFs for each SN ($\sum_k P_{k'}(i)$). In a previous analysis of 94 SNRs (DR18), the stacked age distribution clearly exhibited two distributions: one associated with the progenitors and one associated with random unassociated bursts of star formation. The stacked distribution of DR18 also showed similar features in the progenitor age distribution, namely a clear t_{\max} (hence M_{\min}) and a clear smooth distribution below that t_{\max} . While the number of SNe in this sample is lower than the DR18 study (e.g., 22 SNe vs. 94 SNRs), the stacked distribution in Figure 3 shows similar features to those in DR18, although a little less clear. The most obvious feature

is a reduction in the stacked distribution around 35-45 Myr; which likely reflects the maximum age (i.e., minimum mass) of the progenitor distribution.

Section 2.4 of DR18 derived the progenitor age distribution model considering the SF in each age bin, i , as independent bursts of SF. For simplicity, DR18 considered a power-law distribution ($\frac{dN}{dt} \propto t^\beta$) with a t_{\min} , t_{\max} , and slope (β) in between. Since the stacked distribution in Figure 3 seems consistent with the stacked distribution in DR18, we adopt the same power-law model as in DR18. The primary difference is that we set t_{\min} to a fixed value in this study. Hence, our model only depends upon two parameters, t_{\max} and power-law slope β .

We fixed the t_{\min} parameter because the SFR for the younger age bins are highly uncertain, and these uncertainties are estimates based upon a hybridMC (Dolphin 2013). The large uncertainties on the younger age bins limit the accuracy in inferring t_{\min} . The approximate nature of the hybridMC compounds this problem. Hence, there is not enough information in this sample to effectively constrain both t_{\min} and the power-law slope β simultaneously. For simplicity, we

Table 2. Conditions for the prior distributions.

Parameter	Prior
Minimum age t_{\min}	$\mathcal{U}(5.62 \text{ Myr}, t_{\max})^1$
Maximum age t_{\max}	$\mathcal{U}(5.62 \text{ Myr}, T_{\max})^2$
Slope β	$\mathcal{U}(-1, 10)$

¹ The posterior distributions of t_{\max} and β are insensitive to the choice of t_{\min} . We fix t_{\min} to 5.62 Myr.

² We only considered the SNe with non-zero SF within the last $T_{\max} = 80$ Myr.

only infer t_{\max} and β because we are more certain about the uncertainties for the higher age bins.

Figures 1 and 2 often show multiple bursts of SF for each SN. Presumably one is associated with the progenitor and the other are random unassociated bursts of SF. Therefore, we use the likelihood model of DR18, in which the true age of each SF burst, \hat{t} , is drawn from the power-law (progenitor) distribution or random uniform distribution, $P_p(\hat{t}|\theta)$ and $P_u(\hat{t})$ respectively. We defined the expressions for these two likelihoods in DR18 (see Equation 6 and 7 for more details). For each SN, the likelihood for the SFH is $\mathcal{L}_{k'}(\{\text{SFH}\}|\theta) = \mathcal{L}_{k'}(\{i\}|\theta)$ and the final reduced likelihood is

$$\mathcal{L}_{k'}(\{i\}|\theta) = C \cdot T_{\max} \cdot \sum_{j=1}^{N_{\text{SNe}}} P_{k'}(j) \cdot P_p(j|\theta), \quad (6)$$

see Section 2.5 of DR18 for a full description of this technique. Finally, the posterior distribution for the model parameters is proportional to:

$$P(\theta|\{\text{SFH}\}) \propto \mathcal{L}(\{\text{SFH}\}|\theta) \cdot P(\theta). \quad (7)$$

Using Equation 3 we infer the final posterior distribution, $P_r(\theta|\{\text{CMD}_{k'}\})$ for each r th subsample using emcee. Emcee is a python implementation (Foreman-Mackey et al. 2013, 2019) of the Affine Invariant Markov chain Monte Carlo Ensemble sampler by Goodman & Weare (2010). For this analysis, we use 100 walkers, 200 steps each, and we burn 100 of those. We use 200 steps because we noticed that it always converged to the most likely value using less than 100 steps. The resulting acceptance fraction for this inference is on average around $a_f = 0.625$. The acceptance fraction represents the fraction of proposed steps that were accepted during the sampling (Foreman-Mackey et al. 2013).

Table 2 shows the constraints for the prior distributions, $P(\theta)$. For this study, the prior distribution is $P(\theta) = P(t_{\max}) \cdot P(\beta)$.

3 RESULTS

The posterior distribution for the maximum age, t_{\max} , and power-law slope for the age distribution, β , are shown in Figure 4. While the proposed age distribution model also depends upon a minimum age (t_{\min}), we do not infer its value; rather, we fix it to 5.62 Myr as discussed below.

Figures 5a and 5b show β and t_{\max} inferences as a function of the minimum age, t_{\min} . The SFHs are calculated using logarithmic spaced age bins, and the youngest edge of the minimum age bin correspond to $\log_{10}(t/\text{yr}) = 6.6$. The right

panel of Figure 5 shows that all inferences for t_{\max} are consistent within the confidence intervals. However, the confidence intervals for t_{\max} are much larger for $t_{\min} < 5.62$ Myr. This is due to the large variation in SFH at the young age bins (see Figure 1 and Figure 2) and complexities of the evolution of massive stars. On the other hand, the inferences for β (left panel in Figure 5) show that β is significantly different for inferences where $t_{\min} < 5.62$ Myr. Since we know that the older age bins are more certain than the younger age bins, this suggests that t_{\min} should not be less than 5.62 Myr. Hence, for the rest of the analysis, we fix t_{\min} to $\log_{10}(t_{\min}/\text{yr}) = 6.75$; this is $t_{\min} = 5.62$ Myr.

It is impossible to do a t_{\min} sensitivity analysis with the SFH associated with SN192M and SN2005af. In the range between 0 – 50 Myr, both only have one burst of SF in the youngest age bin. Omitting age bins younger than 5.62 Myr for those two cases and calculating the likelihood gives precisely zero. Therefore, it is impossible to do the t_{\min} sensitivity study when including these two SNe. For that reason, we omit these two SNe for our entire analysis resulting in $N_{\text{SNe}} = 22$.

The marginalized values for the age distribution parameters are as follows. The t_{\max} is $35.1^{+4.1}_{-3.0}$ Myr and the power-law slope for the age distribution is $\beta = 0.13^{+0.83}_{-0.74}$. The uncertainties reported for both parameters correspond to the narrowest 68 % confidence interval.

3.1 Age-to- M_{ZAMS}

The main scientific goal for this paper is to understand which stars explode. However, our data is the SFH of the resolved stars within 50 pc around the location of each SN. Hence, we first infer the progenitor age distribution given the SFHs, which then must be translated into a progenitor mass distribution. We do this by applying an age-to- M_{ZAMS} mapping to obtain the progenitor mass distribution shown in Figure 6. In mass space, t_{\max} translates to a M_{\min} and β translates to a power-law slope of α .

The mapping from age to mass requires a few assumptions. We assume solar metallicity and that these progenitors are single-stars. Hence, to map the progenitor age distribution to a progenitor mass distribution, we use stellar evolution models from Marigo et al. (2017). To obtain the distributions for the M_{\min} in Figure 6, we first use the stellar evolution models to find an age vs. mass relationship; see Figure 8 of DR18. We then use this age vs. mass to find an M_{\min} for each t_{\min} in the MCMC step distribution. To infer the power-law slope in mass, we use the chain rule to convert the age distribution to a mass distribution. In terms of β (the power-law slope in age) and γ (the power-law slope in the age to mass function), the power-law slope in mass is $\alpha = -2.61^{+1.05}_{-1.18}$. To find the distribution of α , we evaluate this formula for each β in the MCMC chain. See section 3 of DR18 for details.

Assuming that all these historic SNe resulted from the explosion of single stars, the marginalized mass distribution model parameters are $M_{\min} = 8.60^{+0.37}_{-0.41} M_{\odot}$ and the slope of the progenitor distribution is $\alpha = -2.61^{+1.05}_{-1.18}$. The posterior distributions for the mass distribution parameters are in Figure 6.

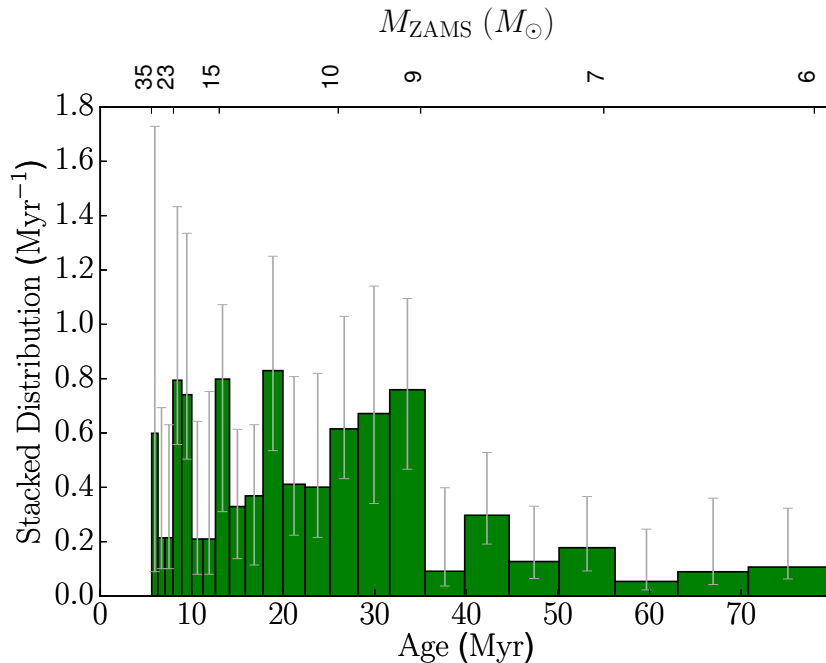


Figure 3. Stacked age distribution for the SN sample shown in Table 1. For each historic SN, we derived a probability distribution from the individual SFHs; see Equation (5). We then sum those distributions to construct an age distribution for all SNe in our sample. Similar to Díaz-Rodríguez et al. (2018), we model this distribution using two components. Component one represents a power-law distribution with a slope of β , a minimum age, t_{\min} , and a maximum age, t_{\max} . In this analysis, we fix t_{\min} due to the low number of SNe in this analysis and highly uncertain SFR for young age bins. The second component is an underlying uniform distribution that represents random unassociated bursts of star formation.

4 DISCUSSION & CONCLUSION

Using a Bayesian hierarchical model previously derived in DR18, we infer the progenitor age distribution for 22 historic CCSNe. We use the SFH for nearby stars ($r < 50\text{pc}$) as a proxy for the age distribution for each SN. The SFHs for 11 of the SNe were previously published in W14, and the remaining 11 SFHs are from W18. We infer a t_{\max} for CCSNe of $t_{\max} = 35.1^{+4.1}_{-3.0}$ Myr and a power-law slope for the progenitor age distribution of $\beta = 0.13^{+0.83}_{-0.74}$, while fixing the minimum age to $t_{\min} = 5.62$ Myr (see Figure 4). Under the assumption that all progenitors were single stars, the age distribution translates to a progenitor mass distribution with a minimum mass of $M_{\min} = 8.60^{+0.37}_{-0.41} M_{\odot}$ and a slope of $\alpha = -2.61^{+1.05}_{-1.18}$ (see Figure 6). Both the M_{\min} and power-law slope α are consistent within uncertainty with previous studies using the direct-imaging and age-dating techniques (see Figure 7). This study is also consistent with progenitor studies using metal abundance study of Galactic SNRs (Katsuda et al. 2018).

4.1 Minimum Mass for CCSNe

Predicting the exact value for the M_{\min} is not trivial and it depends upon a variety of factors such as metallicity, binary interactions, mixing processes, rotation, etc. (e.g., Eldridge & Tout 2004; Ibeling & Heger 2013; Doherty et al. 2015; Zapartas et al. 2017). Ibeling & Heger (2013) studied the minimum initial mass for classical CCSNe as a function of metallicity, Z , using non-rotating models. In this study, they found a mass limit of $\sim 8.35 M_{\odot}$ at $Z = -2.3$ and a limit

of $\sim 9.5 M_{\odot}$ at $Z = 0$. Moreover, they found that the initial mass limit continued to rise with higher metallicity. They also found that for a fixed initial mass function, the SN rate is 20% - 25% higher at low metallicity. In addition to this, various studies have shown that the convective overshooting parameter can affect the minimum initial mass values for an SN. This extra mixing is used to simulate any mixing process and not just convective overshooting, like rotation or gravity wave mixing (Eldridge & Tout 2004). Essentially, a higher convective overshooting parameter and low metallicity will generally shift the M_{\min} to lower values (Eldridge & Tout 2004; Podsiadlowski et al. 2004).

It is difficult to constrain the progenitors of CCSNe, because only a few of them have been discovered directly, making the statistical constraints quite loose. W18 inferred the progenitor masses for 25 historic CCSNe (SN sample used in this work + 3 SN) using the SFHs near each SN. They found that the sample is consistent with a M_{\min} for CCSNe of $< 9.5 M_{\odot}$ (90% confidence). In this study, we determine an initial mass of $M_{\min} = 8.60^{+0.37}_{-0.41} M_{\odot}$ for 22 historic SNe. The RSG sample (Smartt 2015) and the Historic SN sample from this study gives consistent results within a 68% confidence interval (see Figure 7). On the other hand, the SNR sample (DR18) is only consistent at the 2-sigma level. More upcoming data will determine whether this slight inconsistency is a result due to a small sample size or some physical bias. If the inconsistency persists, then it could be due to several factors. For one, the M_{\min} might be a function of metallicity as other studies have shown (e.g. Eldridge & Tout 2004; Podsiadlowski et al. 2004). The Historic SN and

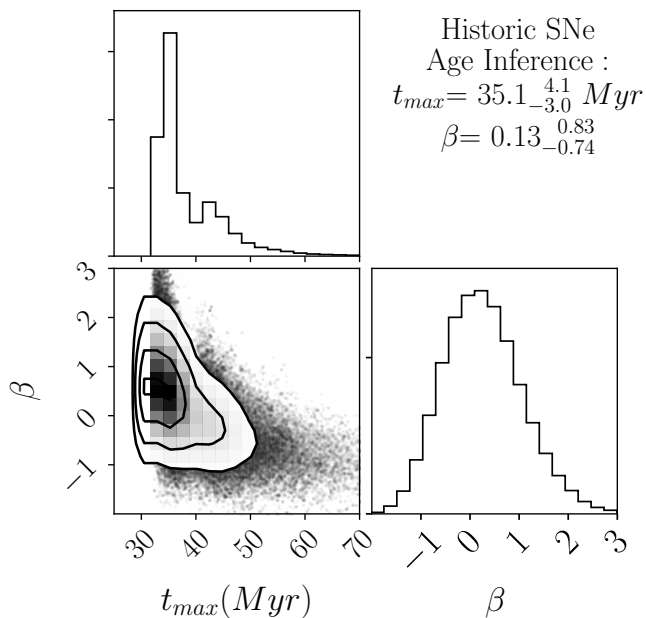


Figure 4. Posterior distribution for the model parameters of the age distribution: the maximum age is t_{\max} , and the power-law slope is β . We fixed the minimum age in our inference to be $t_{\min} = 5.62$ Myr. The mode and narrowest 68% confidence interval for the parameters are $t_{\max} = 35.1_{-3.0}^{+4.1}$ Myr and $\beta = 0.13_{-0.74}^{+0.83}$.

RSG samples represent a heterogeneous metallicity sample, whereas, the SNR sample comes from two particular galaxies and presumably a narrower range of metallicity. Another possible explanation is that SNRs are biased toward older ages (hence smaller masses). Therefore, a definitive resolution will require more progenitor stars. Binary evolution may also affect progenitor mass distribution inferences for SNe (de Mink et al. 2014). There are two ways in which binary evolution may affect age estimates. For one, mass transfer from one star to another can alter the relationship between zero-age-main sequence mass and age. For instance, Zapartas et al. (2019) found that approximately 33% to 50% of Type II SN progenitors had exchange mass with a companion before exploding for most model assumptions. For example, two $4 M_{\odot}$ stars could merge when one evolves off of the MS. The age of these stars and surrounding population would correspond to the age of a $4 M_{\odot}$ star near its death, yet it would explode as an $8 M_{\odot}$ star. In this scenario, the surrounding population is much older than the single star scenario would allow. In the second case, when one of the binary stars explodes, the companion could be ejected at a high velocity. As a consequence, the star that was kicked out could eventually explode in an older region.

If one does not account for binarity, the initial mass inferred for binary stars could be overestimated by 15-25% than its true initial mass (Zapartas et al. 2020). Further illustrating a need to consider binary evolution, the sample in this study contains four Type Ib/c SNe that have a wide range of ages (W18). Hence, W18 suggested that this result is consistent with a large fraction of SN Ib/c originating from binary evolution. While these previous investigations motivate a need

for including binary evolution in inferring ages, we use single star models in this analysis to provide a baseline for comparison.

4.2 Mass Distribution Power-Law Slope

We find a power-law slope of $\alpha = -2.61_{-1.18}^{+1.05}$ for the progenitor mass distribution. This value is consistent with the standard Salpeter IMF ($dN/dM \propto M^{\alpha}$, where $\alpha = -2.35$). Both our inferred parameters, M_{\min} and α , are consistent within the uncertainties of previous progenitor estimates using direct detections and the age-dating technique (Smartt 2015; Jennings et al. 2014; Williams et al. 2018). W18 estimated the masses for 25 CCSNe (22 of these are considered in this study) and found that the progenitor mass distribution is consistent with a Salpeter IMF distribution as well. DR18 found a steeper slope of $\alpha = -2.96_{-0.25}^{+0.45}$ using 94 SNRs in M31 and M33 (see Figure 7). The results of DR18 suggest that either the most massive stars are not exploding as frequently as lower mass stars, or there is a bias against observing SNRs in the youngest regions. While those results prefer a slight steeper distribution, and the results of this paper are consistent with a Salpeter IMF, both are consistent with one another. For the most part, this is because the confidence interval of this study is larger.

ACKNOWLEDGEMENTS

Based on observations made with the NASA/ESA Hubble Space Telescope, obtained [from the Data Archive] at the Space Telescope Science Institute, which is operated by the Association of Universities for Research in Astronomy, Inc., under NASA contract NAS 5-26555. Support for programs # HST-AR-13882, # HST-AR-15042, and # HST-GO-14786 was provided by NASA through a grant from the Space Telescope Science Institute, which is operated by the Association of Universities for Research in Astronomy, Inc., under NASA contract NAS 5-26555.

REFERENCES

- Auchettl K., Lopez L. A., Badenes C., Ramirez-Ruiz E., Beacom J. F., Holland -Ashford T., 2019, *ApJ*, **871**, 64
 Badenes C., Harris J., Zaritsky D., Prieto J. L., 2009, *The Astrophysical Journal*, **700**, 727
 Badenes C., Maoz D., Ciardullo R., 2015, *ApJ*, **804**, L25
 Beasar E. R., Davies B., 2016, *MNRAS*, **463**, 1269
 Bovy J., 2016, *ApJ*, **817**, 49
 Burrows A., Goshy J., 1993, *ApJ*, **416**, L75
 Colquhoun D., 2014, *Royal Society open science*, **1**, 140216
 Crockett R. M., et al., 2008, *MNRAS*, **391**, L5
 Davies B., Beasar E. R., 2018, *Monthly Notices of the Royal Astronomical Society*, **474**, 2116
 Davies B., Beasar E. R., 2020, *MNRAS*, **493**, 468
 Díaz-Rodríguez M., Murphy J. W., Rubin D. A., Dolphin A. E., Williams B. F., Dalcanton J. J., 2018, *ApJ*, **861**, 92
 Doherty C. L., Gil-Pons P., Siess L., Lattanzio J. C., Lau H. H. B., 2015, *MNRAS*, **446**, 2599
 Dolphin A. E., 2000, *PASP*, **112**, 1383
 Dolphin A. E., 2002, *MNRAS*, **332**, 91
 Dolphin A. E., 2012, *ApJ*, **751**, 60
 Dolphin A. E., 2013, *ApJ*, **775**, 76

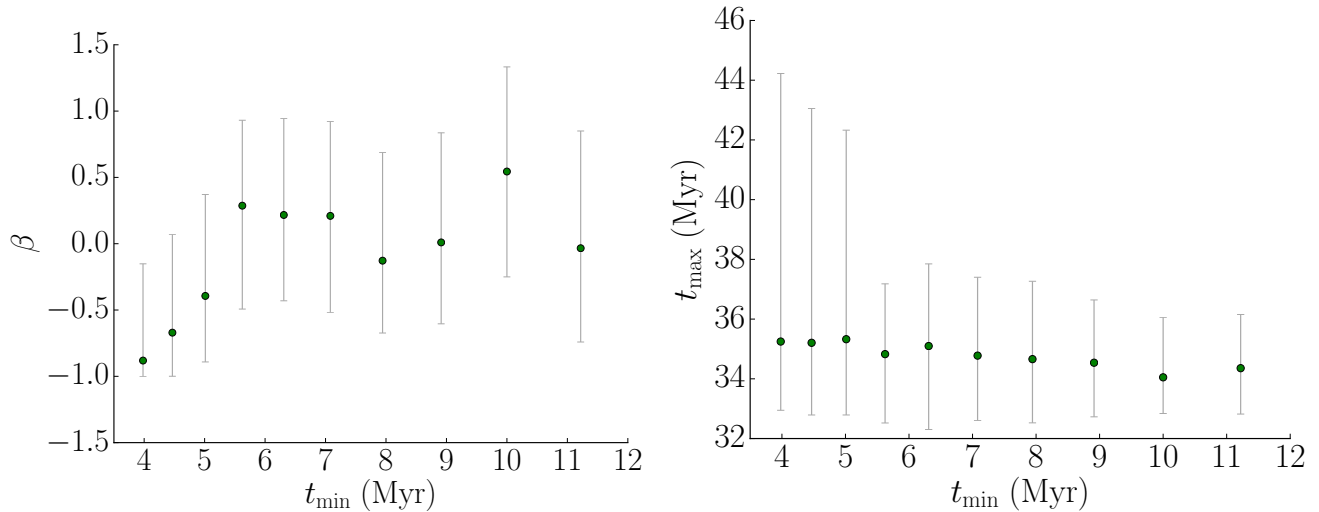


Figure 5. Inferred model parameters as a function of minimum age, t_{\min} . The green dots represent the mode for β and t_{\max} , and the gray bars represent the narrowest 68% confidence interval for the uncertainty. Below $t_{\min} < 5.62$ Myr the inference for β is not stable; above it is. Since the uncertainties are largest and least certain at the youngest ages, we restrict our analysis to age above 5.62 Myr. On the other hand, the inferences for t_{\max} are mostly consistent for all trials of t_{\min} . For $t_{\min} < 5.62$ Myr, the confidence interval for t_{\max} are much larger. This is largely due to the uncertainties in the SFH at young age bins. For these reasons, we set t_{\min} age bin to 5.62 Myr for the rest of the analysis.

- Dolphin A., 2016, DOLPHOT: Stellar photometry, Astrophysics Source Code Library (ascl:1608.013)
- Dolphin A. E., et al., 2003, *AJ*, **126**, 187
- Ebinger K., Curtis S., Fröhlich C., Hempel M., Perego A., Liebendörfer M., Thielemann F.-K., 2018, *The Astrophysical Journal*, **870**, 1
- Eldridge J. J., Tout C. A., 2004, *MNRAS*, **353**, 87
- Farrell E. J., Groh J. H., Meynet G., Eldridge J. J., 2020, *MNRAS*, **494**, L53
- Foreman-Mackey D., Hogg D. W., Lang D., Goodman J., 2013, *PASP*, **125**, 306
- Foreman-Mackey D., et al., 2019, *The Journal of Open Source Software*, **4**, 1864
- Fraser M., et al., 2014, *MNRAS*, **439**, L56
- Gal-Yam A., Leonard D. C., 2009, *Nature*, **458**, 865
- Gallart C., Zoccali M., Aparicio A., 2005, *ARA&A*, **43**, 387
- Girardi L., et al., 2010, *ApJ*, **724**, 1030
- Gogarten S. M., Dalcanton J. J., Murphy J. W., Williams B. F., Gilbert K., Dolphin A., 2009, *ApJ*, **703**, 300
- Goodman J., Weare J., 2010, *Communications in Applied Mathematics and Computational Science*, Vol. 5, No. 1, p. 65-80, **2010**, **5**, 65
- Hendry M. A., et al., 2006, *MNRAS*, **369**, 1303
- Ibeling D., Heger A., 2013, *ApJ*, **765**, L43
- Jennings Z. G., Williams B. F., Murphy J. W., Dalcanton J. J., Gilbert K. M., Dolphin A. E., Foesneau M., Weisz D. R., 2012, *ApJ*, **761**, 26
- Jennings Z. G., Williams B. F., Murphy J. W., Dalcanton J. J., Gilbert K. M., Dolphin A. E., Weisz D. R., Foesneau M., 2014, *ApJ*, **795**, 170
- Katsuda S., Takiwaki T., Tominaga N., Moriya T. J., Nakamura K., 2018, *ApJ*, **863**, 127
- Kochanek C. S., 2020, *MNRAS*, **493**, 4945
- Lada C. J., Lada E. A., 2003, *ARA&A*, **41**, 57
- Leonard D. C., 2010, in Leitherer C., Bennett P. D., Morris P. W., Van Loon J. T., eds, *Astronomical Society of the Pacific Conference Series Vol. 425, Hot and Cool: Bridging Gaps in Massive Star Evolution*. p. 79 ([arXiv:0908.1812](https://arxiv.org/abs/0908.1812))
- Lewis A. R., et al., 2015, *ApJ*, **805**, 183
- Li W., Van Dyk S. D., Filippenko A. V., Cuillandre J.-C., 2005, *PASP*, **117**, 121
- Li W., Van Dyk S. D., Filippenko A. V., Cuillandre J.-C., Jha S., Bloom J. S., Riess A. G., Livio M., 2006, *ApJ*, **641**, 1060
- Li W., Wang X., Van Dyk S. D., Cuillandre J.-C., Foley R. J., Filippenko A. V., 2007, *ApJ*, **661**, 1013
- Mabanta Q. A., Murphy J. W., 2018, *ApJ*, **856**, 22
- Maíz-Apellániz J., Bond H. E., Siegel M. H., Lipkin Y., Maoz D., Ofek E. O., Poznanski D., 2004, *ApJ*, **615**, L113
- Marigo P., et al., 2017, *ApJ*, **835**, 77
- Maund J. R., 2017, *MNRAS*, **469**, 2202
- Maund J. R., 2018, *MNRAS*, **476**, 2629
- Maund J. R., Smartt S. J., Kudritzki R. P., Podsiadlowski P., Gilmore G. F., 2004, *Nature*, **427**, 129
- Maund J. R., Smartt S. J., Danziger I. J., 2005, *MNRAS*, **364**, L33
- Maund J. R., et al., 2011, *ApJ*, **739**, L37
- Maund J. R., Mattila S., Ramirez-Ruiz E., Eldridge J. J., 2014, *MNRAS*, **438**, 1577
- Murphy J. W., Burrows A., 2008, *ApJ*, **688**, 1159
- Murphy J. W., Dolence J. C., 2017, *ApJ*, **834**, 183
- Murphy J. W., Jennings Z. G., Williams B., Dalcanton J. J., Dolphin A. E., 2011, *ApJ*, **742**, L4
- Murphy J. W., Khan R., Williams B., Dolphin A. E., Dalcanton J., Díaz-Rodríguez M., 2018, *ApJ*, **860**, 117
- Panagia N., Romaniello M., Scuderi S., Kirshner R. P., 2000, *ApJ*, **539**, 197
- Podsiadlowski P., Langer N., Poelarends A. J. T., Rappaport S., Heger A., Pfahl E., 2004, *ApJ*, **612**, 1044
- Sarbadhicary S. K., Badenes C., Chomiuk L., Caprioli D., Huizenga D., 2017, *MNRAS*, **464**, 2326
- Smartt S. J., 2009, *ARA&A*, **47**, 63
- Smartt S. J., 2015, *Publ. Astron. Soc. Australia*, **32**, e016
- Smartt S. J., Gilmore G. F., Tout C. A., Hodgkin S. T., 2002a, *ApJ*, **565**, 1089
- Smartt S. J., Vreeswijk P. M., Ramirez-Ruiz E., Gilmore G. F., Meikle W. P. S., Ferguson A. M. N., Knapen J. H., 2002b, *ApJ*, **572**, L147

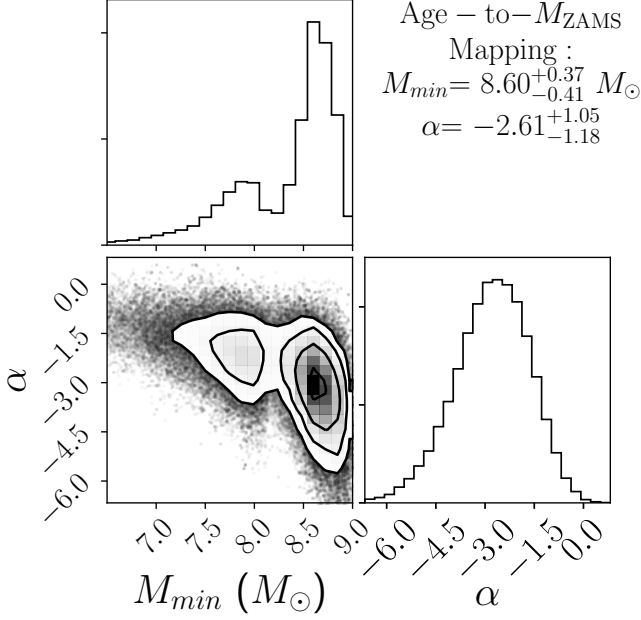


Figure 6. Posterior distribution for the progenitor-mass distribution parameters. Using a mapping between age and mass for single star evolution, we transform the posterior distribution for t_{\max} and β (Figure 4) to a posterior distribution for M_{\min} and α . The minimum mass is $M_{\min} = 8.60^{+0.37}_{-0.41} M_{\odot}$ and the slope is $\alpha = -2.61^{+1.05}_{-1.18}$. The power-law index inferred in this analysis is consistent with the inference of Díaz-Rodríguez et al. (2018) which used 94 supernova remnants (SNRs), while the M_{\min} is consistent within the 95% confidence interval (see Figure 7). The large uncertainty for α is consistent with a wide range of distributions, including Salpeter and the steep power-law inferred from the SNRs.

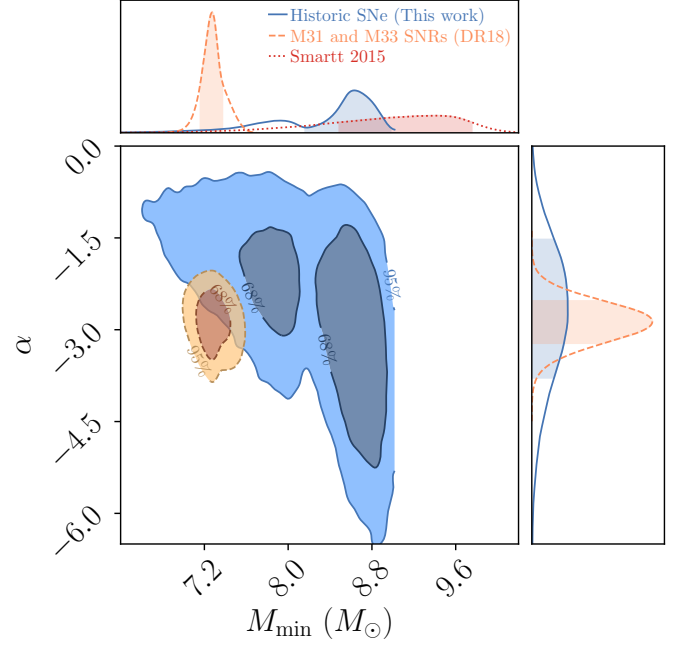


Figure 7. Posterior distribution for the progenitor-mass distribution parameters. This figure compares the results for this work (Figure 6, blue contour) with previous progenitor mass distribution inferences. The orange contour shows the results of DR18, which inferred the distribution using 94 supernova remnants for M31 and M33. The red distribution in the top panel shows the distribution from 26 type II SN (mostly type II-P) (Smartt 2015). The power-law index (α) for both this and the DR18 studies are consistent with each other, while the M_{\min} inferred for the SNRs is slightly lower than the inference using the historic SNe. The Smartt (2015) analysis has relatively large uncertainties and is formally consistent with both age-dating inferences.

Smartt S. J., Maund J. R., Hendry M. A., Tout C. A., Gilmore G. F., Mattila S., Benn C. R., 2004, *Science*, **303**, 499
 Smartt S. J., Eldridge J. J., Crockett R. M., Maund J. R., 2009, *MNRAS*, **395**, 1409
 Smith N., et al., 2011, *ApJ*, **732**, 63
 Sukhbold T., Ertl T., Woosley S. E., Brown J. M., Janka H.-T., 2016, *ApJ*, **821**, 38
 Ugliano M., Janka H.-T., Marek A., Arcones A., 2012, *ApJ*, **757**, 69
 Van Dyk S. D., 2017, *RSPTA*, **375**, 20160277
 Van Dyk S. D., Li W., Filippenko A. V., 2003a, *PASP*, **115**, 448
 Van Dyk S. D., Li W., Filippenko A. V., 2003b, *PASP*, **115**, 1289
 Van Dyk S. D., et al., 2011, *ApJ*, **741**, L28
 Van Dyk S. D., et al., 2012a, *AJ*, **143**, 19
 Van Dyk S. D., et al., 2012b, *ApJ*, **756**, 131
 Vinkó J., et al., 2009, *ApJ*, **695**, 619
 Walmswell J. J., Eldridge J. J., 2012, *MNRAS*, **419**, 2054
 Wang X., Yang Y., Zhang T., Ma J., Zhou X., Li W., Lou Y.-Q., Li Z., 2005, *ApJ*, **626**, L89
 Williams B. F., Peterson S., Murphy J., Gilbert K., Dalcanton J. J., Dolphin A. E., Jennings Z. G., 2014, *ApJ*, **791**, 105
 Williams B. F., Hillis T. J., Murphy J. W., Gilbert K., Dalcanton J. J., Dolphin A. E., 2018, *The Astrophysical Journal*, **860**, 39
 Williams B. F., Hillis T. J., Blair W. P., Long K. S., Murphy J. W., Dolphin A., Khan R., Dalcanton J. J., 2019, *ApJ*, **881**, 54
 Woosley S. E., Heger A., Weaver T. A., 2002, *Reviews of Modern Physics*, **74**, 1015
 Zapartas E., et al., 2017, *A&A*, **601**, A29

Zapartas E., et al., 2019, *A&A*, **631**, A5
 Zapartas E., de Mink S. E., Justham S., Smith N., Renzo M., de Koter A., 2020, arXiv e-prints, p. arXiv:2002.07230
 de Mink S. E., Sana H., Langer N., Izzard R. G., Schneider F. R. N., 2014, *ApJ*, **782**, 7